HHS Public Access

Author manuscript

Phys Med Biol. Author manuscript; available in PMC 2016 March 21.

Published in final edited form as:

Phys Med Biol. 2015 March 21; 60(6): 2309–2324. doi:10.1088/0031-9155/60/6/2309.

Reconstruction of Organ Dose for External Radiotherapy Patients in Retrospective Epidemiologic Studies

Choonik Lee[1], **Jae Won Jung**[2], **Christopher Pelletier**[2], **Anil Pyakuryal**[3], **Stephanie Lamart**[3], **Jongoh Kim**[4], and **Choonsik Lee**[3]

[1]Department of Radiation Oncology, University of Michigan, Ann Arbor, MI

[2]Department of Physics, East Carolina University

[3]Division of Cancer Epidemiology and Genetics, National Cancer Institute, National Institute of Health, Rockville, MD

[4]Radiation Oncology, University of Pittsburg Cancer Institute

Abstract

Organ dose estimation for retrospective epidemiological studies of late effects in radiotherapy patients involves two challenges: radiological images to represent patient anatomy are not usually available for patient cohorts who were treated years ago, and efficient dose reconstruction methods for large-scale patient cohorts are not well established. In the current study, we developed methods to reconstruct organ doses for radiotherapy patients by using a series of computational human phantoms coupled with a commercial treatment planning system (TPS) and a radiotherapy-dedicated Monte Carlo transport code, and performed illustrative dose calculations. First, we developed methods to convert the anatomy and organ contours of the pediatric and adult hybrid computational phantom series to Digital Imaging and Communications in Medicine (DICOM)-image and DICOM-structure files, respectively. The resulting DICOM files were imported to a commercial TPS for simulating radiotherapy and dose calculation for in-field organs. The conversion process was validated by comparing electron densities relative to water and organ volumes between the hybrid phantoms and the DICOM files imported in TPS, which showed agreements within 0.1% and 2%, respectively. Second, we developed a procedure to transfer DICOM-RT files generated from the Eclipse system directly to a Monte Carlo transport code, X-ray Voxel Monte Carlo (XVMC) for more accurate dose calculations. Third, to illustrate the performance of the established methods, we simulated a whole brain treatment for the 10-year-old male phantom and a prostate treatment for the adult male phantom. Radiation doses to selected organs were calculated using the Eclipse and XVMC, and compared to each other. Organ average doses from the two methods matched within 7%, whereas maximum and minimum point doses differed up to 45%. The dosimetry methods and procedures established in this study will be useful for the reconstruction of organ dose to support retrospective epidemiological studies of late effects in radiotherapy patients.

For reprints and correspondence contact: Choonsik Lee, PhD, Investigator, Radiation Epidemiology Branch, Division of Cancer Epidemiology and Genetics, National Cancer Institute, National Institute of Health, Rockville, MD 20850, Phone: 240-276-7374, leechoonsik@mail.nih.gov.

Keywords

Organ dose reconstruction; Phantom; Radiotherapy; DICOM

1 Introduction

Epidemiological studies of the risk of late effects in radiotherapy patients require dosimetry methods that provide individualized organ-specific radiation doses inside as well as outside of the treatment fields. In most retrospective epidemiological studies, organ doses need to be reconstructed for patients treated many years in the past. Two challenges are involved in this task. First, radiological images representing full patient anatomy are not generally available on the individual level for the patient cohort. In some cases partial scans may be available, but in many cases no image sets exist. Second, efficient dose reconstruction methods for a large-scale patient cohort are not well established.

Different dosimetry methods have been employed in large-scale retrospective epidemiological studies when radiological images are not available. Stovall et al. used various approaches for the organ dose reconstructions of radiotherapy patients (Stovall *et al* 1995, 2004, 2006): derivation of organ average dose using a matrix of point dose measurements within a water phantom under the radiotherapy machines and direct thermo-luminescent dosimeter (TLD) measurements using physical anthropomorphic phantoms. Diallo et al. introduced DOS-Eg software, which is based on a simplified stylistic human anatomy and water phantom measurements, for evaluation of peripheral doses in external radiotherapy patients (Diallo *et al* 1996). This group later developed ICTA software with improved human anatomy based on computed tomography (CT) images (Ligot *et al* 1998). Although these methods have been widely used for numerous epidemiological studies (Stovall *et al* 2006) mainly thanks to the fast computational time, the anatomical models in the existing methods are limited to either simplified water phantoms, which may not accurately take into account the complex and heterogeneous human anatomy, or fixed anatomy segmented from a single individual, which may not represent the anatomy of an entire patient cohort with significant variation in body size.

In the field of medical physics, computational human phantoms have been actively developed to describe human anatomy and to facilitate the calculation of radiation dose to organs and tissues, and widely used for organ dose calculations for reference individuals undergoing a variety of radiation-involved diagnostic and therapeutic procedures. Since the introduction of mathematical (or stylized) phantoms in the 1970s (Cristy and Eckerman 1987), computational phantoms have evolved from a simple format based on mathematical surface equations, to voxel (or tomographic) phantoms based on tomographic images of real patients(Caon 2004, Zaidi and Xu 2007), and more recently to hybrid phantoms where the advantages of the two earlier classes of phantom, the flexibility of stylized and the realism of voxel phantoms, are combined (Xu *et al* 2007, Segars and Tsui 2009, Lee *et al* 2007, Xu 2014). The hybrid phantoms (or boundary representation: BREP) are the most realistic and flexible format of computational phantoms to date. The pediatric hybrid voxel phantom series (Lee *et al* 2010) that were developed under the collaboration between the University

of Florida and the National Cancer Institute were recently adopted as pediatric reference phantoms by the International Commission on Radiological Protection (ICRP).

Several researchers reported new methods coupling the computational human phantoms with Monte Carlo transport codes to calculate organ doses for radiotherapy patients. Bednarz et al. simulated 6 and 18 MV linear accelerators using a Monte Carlo transport code (Bednarz and Xu 2009), and coupled the models with their pregnant women computational phantom to assess fetal doses from 6-MV external photon radiotherapy (Bednarz and Xu 2008). They also employed an adult male whole body phantom to calculate out-of-field organ doses for prostate treatments (Bednarz *et al* 2010, 2009). Athar et al. (Athar *et al* 2010, Athar and Paganetti 2011) reported the comparison of out-of-field photon dose in intensity modulated radiation treatment (IMRT) and neutron dose in proton therapy by using MC transport method and adult and pediatric voxel phantoms. Joosten et al. (Joosten *et al* 2011, 2013) reported organ-specific peripheral doses after IMRT for breast cancer treatments using a whole body CT scan coupled with in-house Monte Carlo model of 6MV beams. Although Monte Carlo calculations were not conducted, Moignier et al. (Moignier *et al* 2013) reported a feasibility to use hybrid computational phantoms for retrospective heart dosimetry after breast radiation therapy by importing hybrid phantoms into a treatment planning system. However, the existing methods may not be readily used for a large-scale epidemiological study because of relatively long computation time in the Monte Carlo calculations and the lack of convenient interface for physicists to perform a treatment planning.

In the current study, we developed an efficient workflow to provide organ dose estimates of radiotherapy patients to support a large-scale retrospective epidemiological study, where patient images are not available. We imported the hybrid phantoms into the existing treatment planning system (TPS), a convenient tool for physicists to perform a treatment planning and organ dose calculation. We also developed a streamlined procedure to conduct Monte Carlo (MC)-based dose calculations by directly importing DICOM-Radiation Treatment (RT) files into a radiotherapy-dedicated Monte Carlo code. We also conducted illustrative applications of the established methods for two cases of cancer treatment using pediatric and adult phantoms.

2 Materials and methods

2.1 Hybrid computational phantom series

We adopted a series of pediatric and adult reference hybrid phantoms (Lee *et al* 2010). The hybrid phantoms have several advantages over the simplified or individualized surrogates adopted by the existing dose calculation methods (Stovall *et al* 2006, Diallo *et al* 1996, Ligot *et al* 1998). First, the organ and tissue masses in the hybrid phantoms matched to the reference masses reported by ICRP(ICRP 2002). The reference alimentary tract dimensions (e.g., the length of small intestine) are employed in the phantom development(ICRP 2006). Also, the reference density and elemental composition reported by the ICRP and ICRU are incorporated into the phantoms (ICRU 1992, ICRP 2002). Second, the organs and tissues in the hybrid phantoms are already indexed with their respective contour and material compositions, which will significantly reduce the laborious effort of contouring the organs

of interest in organ dose calculations. Figure 1 shows the 3D rendering of the hybrid phantom series from newborn to adult.

2.2 Conversion of computational phantoms to DICOM images

We converted the hybrid phantoms into DICOM-image files, which are readable in treatment planning systems. The hybrid phantoms composed of Non-Uniform Rational B-Spline (NURBS) and polygon mesh surfaces (Lee *et al* 2010) were voxelized to voxel phantoms with the resolution of $1 \times 1 \times 3$ mm^3. Reference elemental compositions obtained from ICRU (ICRU 1992)and ICRP (ICRP 2002) publications were assigned to a total of 38 organs and tissues and 35 bone sites. The elemental compositions for water and air were also assigned to gastrointestinal contents and air-filled cavities, respectively. A single set of elemental composition was used for cortical bone across different bone sites, whereas separate values were assigned to spongiosa regions in different bone sites.

We intended to import the resulting DICOM-image files into a commercial treatment planning system (TPS), Eclipse™ (Varian Medical System, Palo Alto, CA). The Eclipse system employs the dose calculation algorithm, Analytical Anisotropic Algorithm (AAA) for photon dose calculation, that anisotropically accounts for tissue inhomogeneity in the three dimensional neighborhood by using radiologic scaling of the dose deposition functions in the beam direction and electron-density-based scaling of the photon scatter kernels (Sievinen *et al* 2005). Because the algorithm uses electron density relative to water (referred to as “electron density” hereafter) for dose calculation, we derived the values for each organ and tissue by using the elemental composition and density assigned to the hybrid phantoms as follows:

$$\rho\left[\frac{e}{cm^3}\right] = \rho\left[\frac{g}{cm^3}\right] \times N_A \times \sum_i \frac{f_i \times Z_i}{A_i} \quad (1)$$

where f_i is the mass fraction, Z_i is the atomic number, A_i is the atomic weight of i^{th} element, and N_A is Avogadro's number. The electron density of the water is 3.343×10^{23} electrons/cm^3.

We then converted the electron densities to Hounsfield Units (HU) using the electron density-to-HU conversion table, which has been clinically commissioned in the Department of Radiation Oncology at the University of Michigan (Table 1). Once HU was assigned to each voxel of the hybrid phantoms, the matrix was exported to a 16-bit DICOM file using DICOMWRITE, a function of the MATLAB™ (The Mathworks, Inc., Natick, MA) Image Processing Toolbox™. Electron density was measured in the Eclipse system after importing the phantoms, and compared with the original values to make sure electron densities are accurately transferred. Organs with a variety of electron densities (0.337 – 1.083) were selected for the comparison from the adult male hybrid phantom: lungs, thymus, spinal cord, thyroid, spleen, trachea, and ears.

2.3 Conversion of organ contours to DICOM-Structure files

Even though the pseudo CT images of the hybrid phantoms can be imported into the Eclipse system, organs of interest must be re-contoured to calculate organ doses. Because the comprehensive number of detailed organs and tissues are already contoured in the hybrid phantom, we developed a method to directly convert the organ contours into DICOM-structure files, which will significantly reduce the time and effort to re-contour organs of interest.

We wrote an in-house script using Rhinoceros™ (McNeel North America, Seattle, WA) software to automatically export organ contours from the original hybrid phantoms described by NURBS and polygon mesh surfaces. The contours were generated with 3 mm resolution in z direction to match that of the DICOM-image files. We found iteratively an optimal resolution of polygon mesh abstracted from the perfect NURBS curves that resulted in reasonable file size. We then converted the contour data into DICOM-structure files that can be directly imported into the Eclipse system. We compared the volumes of selected organs between the original hybrid phantoms and the imported organ contours in the Eclipse system. The selected organs included brain, thyroid, and eyeball in the 10-year-old male phantoms, and prostate, urinary bladder wall and content, gonads, and femoral head in the adult male phantom.

2.4 TPS and Monte Carlo dose calculation

Once the DICOM-image and DICOM-structure files were imported into the Eclipse system, we could conduct treatment planning and organ dose calculations using the convenient graphical user interface (GUI). It is reported that AAA, generally adopted by TPS, is fast but less accurate than MC radiation transport algorithms for dose calculation in inhomogeneous media, especially near bone or lung interfaces, and in structures outside of the primary radiation fields (Howell *et al* 2010, Joosten *et al* 2011, 2013, Wang and Ding 2014).

In addition to the TPS-based calculation method, we also employed a Monte Carlo code, X-ray Voxel Monte Carlo (XVMC)(Fippel 1999) to provide more accurate dose calculations in inhomogeneous media and potentially in out-of-field regions. The XVMC code employs several variance reduction techniques, including photon splitting and electron history repetition, to significantly increase calculation speed without loss of accuracy (Kawrakow and Fippel 2000), which has been verified previously (Krieger and Sauer 2005, Fragoso *et al* 2010). The use of a water composition with different densities instead of detailed elemental composition allows for significant increases in calculation speed (Kawrakow *et al* 1996) although there could be up to 10% dose difference (Chetty *et al* 2007, Siebers *et al* 2000). The cross section data of the XVMC code is mostly based on the ICRU 46 report (ICRU 1992). For electron transport, the simplified scattering approximation suggested by Kawrakow et al. (Kawrakow *et al* 1996) is used. For photon transport, the cross section of Compton scattering is the same as EGS4 code (Nelson *et al* 1985) and the Heitler cross section is used for pair production if the energy of particle is above the cut off energy (Fippel 1999). The code was commissioned for a Varian iX accelerator and the agreement between code calculation and ion chamber measurement for percentage depth dose and off-axis profile in water was within 1%.

MC calculation of organ dose using computational human phantoms normally requires complicated coding to translate the phantoms to a format compatible with a given MC code and to define treatment parameters within the code. It is not practical to perform the process for a large number of subjects typically involved in retrospective epidemiological studies. To streamline the process, we developed a method to directly import the DICOM files including the CT images (DICOM-image), anatomical structure (DICOM-structure), and treatment plan (DICOM-plan) to the XVMC code. We used The Computational Environment for Radiotherapy Research (CERR)(Deasy *et al* 2003), a MATLAB-based software that allows for the visualization and analysis of treatment plans from a variety of treatment planning systems, to import the DICOM files and convert them to MATLAB formatted data (.mat) file type. We developed an in-house MATLAB script to convert the plan from .mat to a 3D density matrix (.dmx), using the HU-to-density table, and the XVMC plan format (.vmc).

2.5 Illustrative dose calculations in brain and prostate tumor treatments

Once it was confirmed that the original anatomy and material information were accurately transferred to the Eclipse system and then to the XVMC code, we conducted organ dose calculations by simulating radiation treatments of brain and prostate tumors in the 10-year-old and adult male phantoms, respectively. Radiation doses were calculated for selected organs in each treatment case by using the Eclipse system and XVMC code.

Radiation treatment plans treating the whole brain and prostate were created within Eclipse using the DICOM images of the 10-year-old and adult male phantoms, respectively. We used two opposed parallel fields of 6 MV beam for the whole brain treatment and seven equally weighted isocentric photon beams of 6 MV for the prostate treatment as illustrations. Multileaf Collimator (MLC) was used for the beam shaping.

The Eclipse system was used to calculate radiation dose to organs of interest: brain, brain stem, thyroid, and eye balls for the brain treatment in the 10-year-old phantom; and prostate, urinary bladder, rectum, gonads, and femoral head for the prostate treatment in the adult male phantom. Using the procedure described above, we also transferred DICOM-RT files from Eclipse directly into XVMC for the MC dose calculation. We used 10^8 photon histories per field in both treatment cases to reduce relative errors in resulting organ doses less than 2 %. The dose calculation was performed using a LINUX computation server built with dual six core 2.93 GHz Intel XEON processors and 12.0 GB RAM. Energy cutoffs of 250 keV and 50 keV were used for electron and photon, respectively, in the MC dose calculations. In both the Eclipse system and XVMC code, we calculated organ absorbed dose and dose volume histogram (DVH). The calculation for the adult male prostate treatment took about 30 minutes in the XVMC code and about 1 minute in the Eclipse system.

3 Results

3.1 Conversion of the hybrid phantoms to DICOM files

First, we converted the hybrid voxel phantoms into DICOM-image files using the electron density-to-HU conversion. Tables 2 and 3 list the calculated electron densities using Eq. 1

for organs and skeleton, respectively. Identical sets of electron density were used for males and females under the age of 10-year. Gender-specific density (ICRP 2002, ICRU 1992)was assigned to the organs and tissues in the 15-year-old and adult phantoms except skeletal density, which is common between the male and female phantoms. Second, we generated DICOM-structure files for selected organs in the hybrid phantoms and imported into the Eclipse system. Figure 2 shows the example axial images of the imported organ contours for (a) thyroid in the 10-year-old male phantom and (b) prostate in the adult male phantom, which are indicated using arrows.

After importing the DICOM files into the Eclipse system, we compared the electron density and the volume of organs between the original hybrid phantoms and the imported DICOM files. Table 4 tabulates the electron density comparison that shows excellent agreements within 0.1% on average. Lungs show the greatest difference of 0.59%. Table 5 shows the volume comparison showing overall good agreements within 2%.

3.2 Illustrative organ dose calculations

Figure 3 shows the two treatment plans for brain (top) and prostate (bottom) in the 10-year-old and adult male phantoms, respectively, performed in the Eclipse system. DVH for the organs of interest in both cases is presented in Figure 4: brain, brainstem, eyeballs, and thyroid in the brain tumor case, and bladder, prostate, femoral heads, rectum, and testes in the prostate tumor case, computed from The Eclipse and XVMC represented by dotted and solid lines, respectively. Organ dose distributions from both calculation methods overall match well because the organs are mostly within or very close to the treatment fields.

Table 6 tabulates the average organ doses, and maximum and minimum point doses in voxels contained within a given organ from the Eclipse and XVMC code. Average organ doses from the two methods match within 7% whereas maximum and minimum point doses differ by up to 45%. The significant differences could be explained by several factors, such as differences in dose calculation algorithms between the Eclipse and XVMC, especially the approximated algorithm in the Eclipse accounting for tissue inhomogeneity as mentioned in Section 2.2. The difference in the minimum point doses are relatively high but the absolute doses are very low, e.g., the minimum dose to the femoral heads, 0.06 Gy in Eclipse and 0.10 Gy in XVMC, are less than 0.2% of the average prostate doses. Although the differences in the minimum and maximum point doses are relatively high, these values are not generally considered in epidemiological studies of second cancer risk, which is normally calculated using average organ doses.

4 Discussion

It should be noted that the dosimetry methods developed in the current study are limited to organs of interest located within or very close to the treatment field. The current model of the linear accelerator (LINAC) in the XVMC code does not account for the leakage and scattered radiations from the accelerator head, which contribute to most of out-of-field dose with minimal contribution from internal scattering within patient (Xu *et al* 2008). We are extending the source model to include additional mechanical components outside the LINAC head such as collimators and housing structures. Rigorous experimental validation

for the out-of-field dose calculations is being conducted by comparing with water phantom measurements in collaboration with the Department of Radiation Oncology at the University of Michigan. The XVMC code is also using a water composition with different densities instead of detailed elemental composition to increase calculation speed (Kawrakow *et al* 1996), which however provides dose difference up to 10% (Chetty *et al* 2007, Siebers *et al* 2000). We are exploring a method to assign elemental compositions to different media according to the HU of CT images.

In spite of the limitation, our method has several advantages compared to the existing dosimetry methods used for epidemiological studies of second cancer risk. First, we adopted the reference pediatric and adult hybrid phantoms based on real patient CT images and the ICRP reference data coupled with the NURBS/polygon mesh format. In most cases of retrospective epidemiological studies where patient CT images are not available, the reference phantoms may be the best surrogate representing average population. Second, the methods and procedures we established are efficient for a large-scale patient cohort. Figure 5 depicts the workflow from the data collection from old medical records to final dose calculations, which we are envisioning. A library of detailed and pre-contoured computational human phantoms are ready to pick from the treatment planning system thanks to the technique to directly import the organ contours of the hybrid phantoms into the treatment planning systems and MC code. Depending on the location of organs and characteristics surrounding the organs, users can choose the TPS or MC calculation methods. We recently published an application of the established method to investigating the variation of stomach doses in patients treated for Hodgkin Lymphoma (Lamart *et al* 2013).

5 Conclusion

We developed methods and procedures to efficiently reconstruct organ doses for radiotherapy patients whose radiological images are not available, which is common in retrospective epidemiological studies. The anatomy and organ contours of the hybrid phantoms were imported to a commercial treatment planning system and Monte Carlo transport code, and used for two illustrative dose calculations simulating brain and prostate cancer patients. The established methods may be useful for several tasks in the study of late effect in radiotherapy patients even beyond organ dose reconstructions: the sensitivity analysis of different parameters involved in treatment and patient to organ doses and the use of dose distribution within organs of interest to improve the risk analysis of second cancer. The DICOM files for the 12 pediatric and adult reference hybrid phantoms that are compatible with commercial treatment planning systems can be made available upon request through a non-disclosure agreement with the corresponding author.

Acknowledgments

This work was supported by the intramural research program of the National Institutes of Health, National Cancer Institute, Division of Cancer Epidemiology and Genetics.This study utilized the high-performance computational capabilities of the Helix Linux computing system at the National Institutes of Health, Bethesda, MD. (http://helix.nih.gov).

References

Athar BS, Bednarz B, Seco J, Hancox C, Paganetti H. Comparison of out-of-field photon doses in 6 MV IMRT and neutron doses in proton therapy for adult and pediatric patients. Phys Med Biol. 2010; 55:2879–91. [PubMed: 20427856]

Athar BS, Paganetti H. Comparison of second cancer risk due to out-of-field doses from 6-MV IMRT and proton therapy based on 6 pediatric patient treatment plans. Radiother Oncol. 2011; 98:87–92. [PubMed: 21159398]

Bednarz B, Athar B, Xu XG. A comparative study on the risk of second primary cancers in out-of-field organs associated with radiotherapy of localized prostate carcinoma using Monte Carlo-based accelerator and patient models. Med Phys. 2010; 37:1987–94. [PubMed: 20527532]

Bednarz B, Hancox C, Xu XG. Calculated organ doses from selected prostate treatment plans using Monte Carlo simulations and an anatomically realistic computational phantom. Phys Med Biol. 2009; 54:5271–86. [PubMed: 19671968]

Bednarz B, Xu XG. A feasibility study to calculate unshielded fetal doses to pregnant patients in 6-MV photon treatments using Monte Carlo methods and anatomically realistic phantoms. Med Phys. 2008; 35:3054–61. Online: http://scitation.aip.org/content/aapm/journal/medphys/35/7/10.1118/1.2938519. [PubMed: 18697528]

Bednarz B, Xu XG. Monte Carlo modeling of a 6 and 18 MV Varian Clinac medical accelerator for in-field and out-of-field dose calculations: development and validation. Phys Med Biol. 2009; 54:N43–N57. [PubMed: 19141879]

Caon M. Voxel-based computational models of real human anatomy: a review. Radiat Environ Biophys. 2004; 42:229–35. [PubMed: 14730450]

Chetty, IJ.; Curran, B.; Cygler, JE.; DeMarco, JJ. Report of the AAPM Task Group No. 105: Issues associated with clinical implementation of Monte Carlo-based photon and electron external beam treatment planning. Med. 2007. Online: http://scitation.aip.org/content/aapm/journal/medphys/34/12/10.1118/1.2795842

Cristy, M.; Eckerman, KF. Specific absorbed fractions of energy at various ages from internal photon sources. Oak Ridge, TN: Oak Ridge National Laboratory; 1987.

Deasy, JO.; Blanco, AI.; Clark, VH. CERR: a computational environment for radiotherapy research. Med Phys. 2003. Online: http://scitation.aip.org/content/aapm/journal/medphys/30/5/10.1118/1.1568978

Diallo I, Lamon A, Shamsaldin A, Grimaud E, de Vathaire F, Chavaudra J. Estimation of the radiation dose delivered to any point outside the target volume per patient treated with external beam radiotherapy. Radiother Oncol. 1996; 38:269–71. Online: http://linkinghub.elsevier.com/retrieve/pii/0167814096017136. [PubMed: 8693110]

Fippel, M. Fast Monte Carlo dose calculation for photon beams based on the VMC electron algorithm. Med Phys. 1999. Online: http://scitation.aip.org/content/aapm/journal/medphys/26/8/10.1118/1.598676

Fragoso M, Wen N, Kumar S, Liu D, Ryu S, Movsas B, Munther A, Chetty IJ. Dosimetric verification and clinical evaluation of a new commercially available Monte Carlo-based dose algorithm for application in stereotactic body radiation therapy (SBRT) treatment planning. Phys Med Biol. 2010; 55:4445–64. [PubMed: 20668343]

Howell RM, Scarboro SB, Kry SF, Yaldo DZ. Accuracy of out-of-field dose calculations by a commercial treatment planning system. Phys Med Biol. 2010; 55:6999. [PubMed: 21076191]

ICRP. Basic anatomical and physiological data for use in radiological protection : reference values ICRP Publ. 89. Ann ICRP. 2002; 32:1–277.

ICRP. Human alimentary tract model for radiological protection ICRP Publ. 100. Ann ICRp. 2006; 36:1–336. Online: http://www.sciencedirect.com/science/article/pii/S014664530600008X. [PubMed: 17188182]

ICRU. Photon, Electron, Proton and Neutron Interaction Data for Body Tissues. Vol. 46. International Commission on Radiation Units and Measurements; 1992.

Joosten A, Bochud F, Baechler S, Levi F, Mirimanoff RO, Moeckli R. Variability of a peripheral dose among various linac geometries for second cancer risk assessment. Phys Med Biol. 2011; 56:5131–51. [PubMed: 21775792]

Joosten, A.; Matzinger, O.; Jeanneret-Sozzi, W.; Bochud, F.; Moeckli, R. Evaluation of organ-specific peripheral doses after 2-dimensional, 3-dimensional and hybrid intensity modulated radiation therapy for breast cancer based on Monte Carlo and convolution/superposition algorithms: Implications for secondary cancer risk asses. Radiother Oncol. 2013. Online: http://www.ncbi.nlm.nih.gov/pubmed/23351844

Kawrakow I, Fippel M. Investigation of variance reduction techniques for Monte Carlo photon dose calculation using XVMC. Phys Med Biol. 2000; 45:2163–83. [PubMed: 10958187]

Kawrakow I, Fippel M, Friedrich K. 3D electron dose calculation using a Voxel based Monte Carlo algorithm (VMC). Med Phys. 1996; 23:445–57. [PubMed: 9157256]

Krieger T, Sauer OA. Monte Carlo- versus pencil-beam-/collapsed-cone-dose calculation in a heterogeneous multi-layer phantom. Phys Med Biol. 2005; 50:859–68. [PubMed: 15798260]

Lamart S, Imran R, Simon SL, Doi K, Morton LM, Curtis RE, Lee C, Drozdovitch V, Maass-Moreno R, Chen CC, Whatley M, Miller DL, Pacak K. Prediction of the location and size of the stomach using patient characteristics for retrospective radiation dose estimation following radiotherapy. Phys Med Biol. 2013; 58:8739–53. [PubMed: 24301086]

Lee C, Lodwick D, Bolch WE. NURBS-based 3D anthropomorphic computational phantoms. Radiat Prot Dosimetry. 2007; 127:227–32. Online: http://rpd.oxfordjournals.org/content/127/1-4/227.full.pdf#page=1&view=FitH. [PubMed: 17567763]

Lee C, Lodwick D, Hurtado J, Pafundi D, Williams JL, Bolch WE. The UF family of reference hybrid phantoms for computational radiation dosimetry. Phys Med Biol. 2010; 55:339–63. [PubMed: 20019401]

Ligot L, Diallo I, Shamsaldin A, Chavaudra J, BonaÎti-Pellié C, de Vathaire F. Individualized phantom based on CT slices and auxological data (ICTA) for dose estimations following radiotherapy for skin haemangioma in childhood. Radiother Oncol. 1998; 49:279–85. Online: http://linkinghub.elsevier.com/retrieve/pii/S0167814098000991. [PubMed: 10075261]

Moignier A, Derreumaux S, Broggio D, Beurrier J, Chea M, Boisserie G, Franck D, Aubert B, Mazeron JJ. Potential of hybrid computational phantoms for retrospective heart dosimetry after breast radiation therapy: a feasibility study. Int J Radiat Oncol Biol Phys. 2013; 85:492–9. Online: http://www.ncbi.nlm.nih.gov/pubmed/22608886. [PubMed: 22608886]

Nelson, W.; Hirayama, H.; Rogers, DWO. The EGS4 Code System, SLAC Report No SLAC-265. 1985.

Segars WP, Tsui B. MCAT to XCAT: The evolution of 4-D computerized phantoms for imaging research. IEEE Trans. 2009; 97:1954–68.

Siebers JV, Keall PJ, Nahum AE, Mohan R. Converting absorbed dose to medium to absorbed dose to water for Monte Carlo based photon beam dose calculations. Phys Med Biol. 2000; 45:983–95. Online: http://stacks.iop.org/0031-9155/45/i=4/a=313. [PubMed: 10795986]

Sievinen, J.; Ulmer, W.; Kaissl, W. AAA photon dose calculation model in Eclipse. Palo Alto, CA: 2005.

Stovall M, Blackwell CR, Cundiff J, Novack DH, Palta JR, Wagner LK, Webster EW, Shalek RJ. Fetal dose from radiotherapy with photon beams: report of AAPM Radiation Therapy Committee Task Group No. 36. Med Phys. 1995; 22:63. [PubMed: 7715571]

Stovall M, Donaldson SS, Weathers RE, Robison LL, Mertens AC, Winther JF, Olsen JH, Boice JD Jr. Genetic effects of radiotherapy for childhood cancer: Gonadal dose reconstruction. Int J Radiat Oncol. 2004; 60:542–52. Online: http://linkinghub.elsevier.com/retrieve/pii/S0360301604004985.

Stovall M, Weathers R, Kasper C, Smith SA, Travis L, Ron E, Kleinerman R. Dose Reconstruction for Therapeutic and Diagnostic Radiation Exposures: Use in Epidemiological Studies. Radiat Res. 2006; 166:141–57. Online: http://www.bioone.org/doi/abs/10.1667/RR3525.1. [PubMed: 16808603]

Wang L, Ding GX. The accuracy of the out-of-field dose calculations using a model based algorithm in a commercial treatment planning system. Phys Med Biol. 2014; 59:N113–28. Online: http://www.ncbi.nlm.nih.gov/pubmed/24925858. [PubMed: 24925858]

Xu XG. An exponential growth of computational phantom research in radiation protection, imaging, and radiotherapy: a review of the fifty-year history. Phys Med Biol. 2014; 59:R233–R302. Online: http://www.ncbi.nlm.nih.gov/pubmed/25144730. [PubMed: 25144730]

Xu XG, Bednarz B, Paganetti H. A review of dosimetry studies on external-beam radiation treatment with respect to second cancer induction. Phys Med Biol. 2008; 53:R193–R241. Online: http://iopscience.iop.org/0031-9155/53/13/R01/fulltext/. [PubMed: 18540047]

Xu XG, Taranenko V, Zhang J, Shi C. A boundary-representation method for designing whole-body radiation dosimetry models: pregnant females at the ends of three gestational periods{\textemdash}RPI-P3,-P6 and-P9. Phys Med Biol. 2007; 52:7023. [PubMed: 18029991]

Zaidi H, Xu XG. Computational anthropomorphic models of the human anatomy: The path to realistic Monte Carlo modeling in radiological sciences. Annu Rev Biomed Eng. 2007; 9:471–500. [PubMed: 17298237]

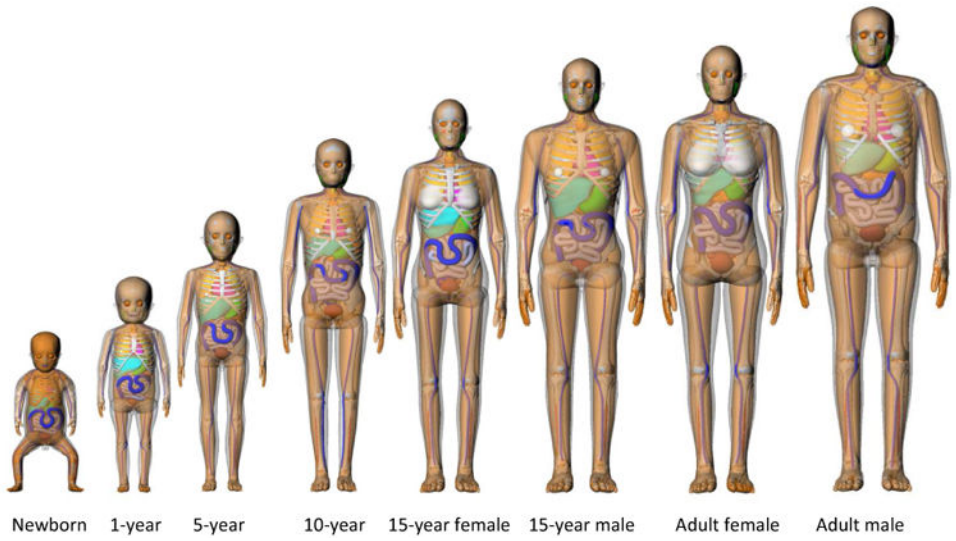

Figure 1.

Series of hybrid phantoms representing pediatric and adult reference individuals. Only male phantoms are visualized for newborn, 1-, 5-, and 10-year-old phantoms because those phantoms share the identical anatomy between male and female except for gender-specific organs.

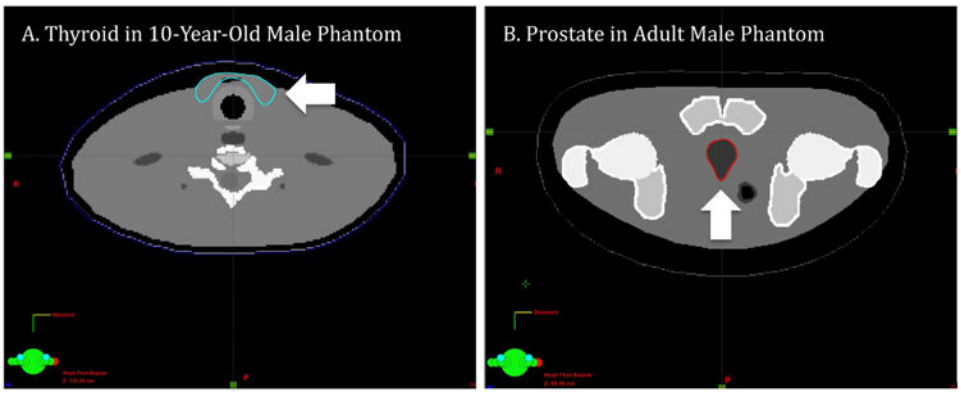

Figure 2.
Examples of the imported organ contours in DICOM-structure files of (a) thyroid in the 10-year-old male phantom and (b) prostate in the adult male phantom (indicated with arrows)

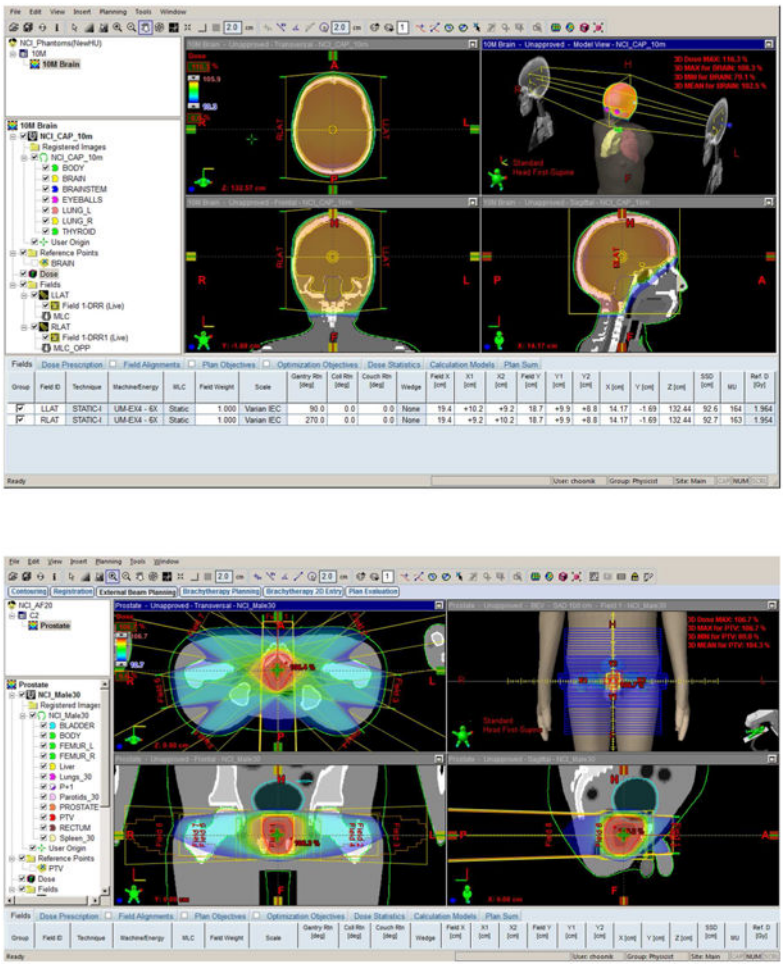

Figure 3.

Treatment plans performed using the Eclipse system for (a) brain and (b) prostate tumors in 10-year-old and adult male phantoms, respectively.

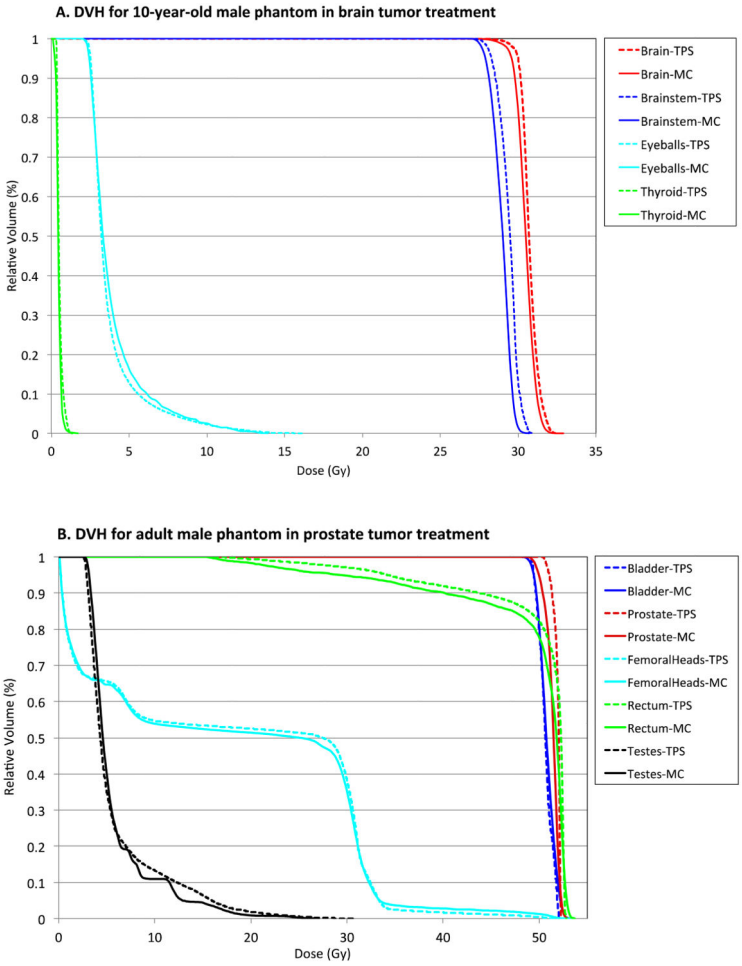

Figure 4.

Comparison of dose volume histogram (DVH) between the Eclipse and XVMC code for tumors and organs of interest in (a) brain tumor treatment of the 10-year-old male phantom and (b) prostate tumor treatment of the adult male phantom.

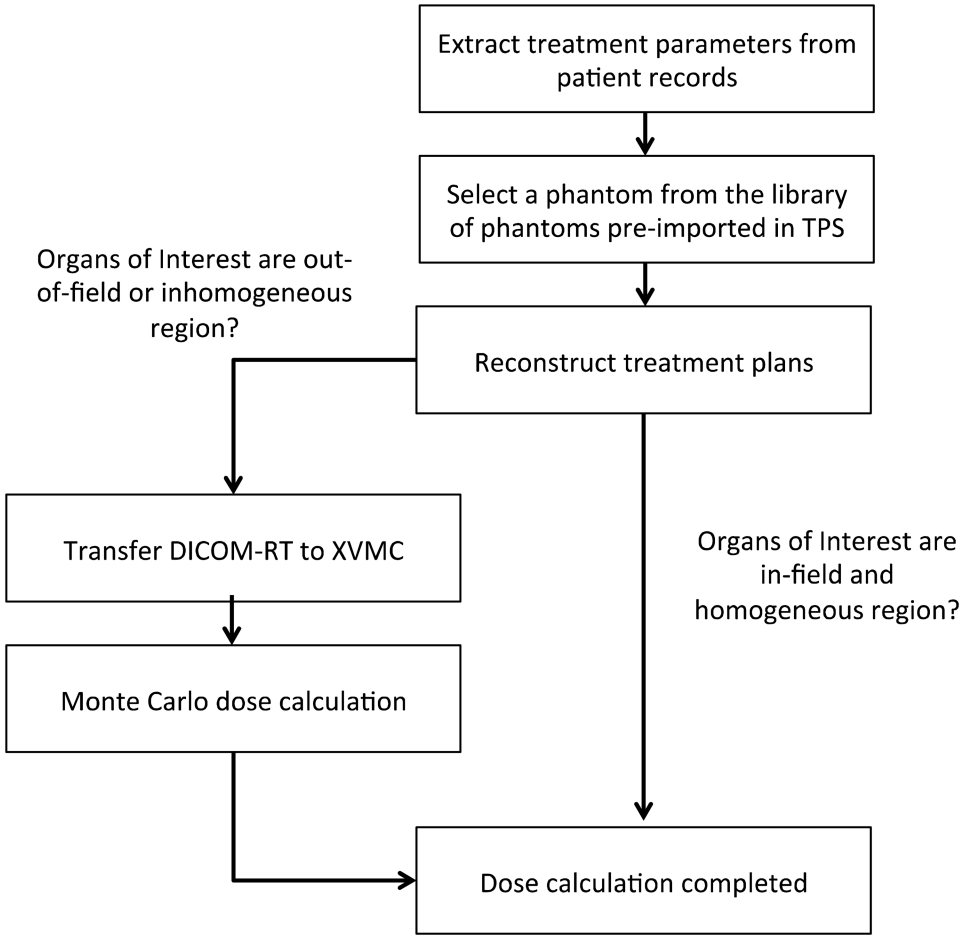

Figure 5.
Diagram showing the workflow of organ dose calculations using the Eclipse system and XVMC code.

Table 1

Electron density to Hunsfield Unit (HU) conversion measured from a reference Computed Tomography phantom.

Relative Electron Density[1]	Hounsfield Unit
0.00	-1000
0.25	-721
0.95	-95
1.00	0
1.64	1000
2.35	1900
5.00	4000

[1] Electron density relative to water

Table 2

Electron density relative to water calculated for organs and tissues included in the hybrid phantom series: 0-, 1-, 5-, 10-, 15-year-old, and adult (AD) male (M) and female (F).

Organs/Tissues	00MF	01MF	05MF	10MF	15F	15M	ADF	ADM
Adrenals	1.025	1.023	1.023	1.023	1.013	1.023	1.013	1.023
Blood	1.039	1.050	1.050	1.050	1.050	1.050	1.050	1.050
Brain	1.023	1.025	1.035	1.035	1.035	1.035	1.035	1.035
Breast glandular	1.014	1.014	1.014	1.014	1.014	1.014	1.014	1.014
Cartilage	1.083	1.083	1.083	1.083	1.083	1.083	1.083	1.083
Epididymis	1.025	1.023	1.023	1.023	1.023	1.023	1.023	1.023
Esophagus	1.025	1.023	1.023	1.023	1.023	1.023	1.023	1.023
Eyes	1.015	1.015	1.015	1.015	1.005	1.015	1.005	1.015
Fat	0.989	0.961	0.961	0.961	0.961	0.961	0.951	0.951
Gall bladder	1.025	1.023	1.023	1.023	1.013	1.023	1.013	1.023
Heart	1.034	1.032	1.032	1.032	1.032	1.032	1.042	1.042
Kidneys	1.025	1.031	1.031	1.031	1.031	1.031	1.041	1.041
Colon	1.024	1.024	1.024	1.024	1.024	1.024	1.024	1.024
Larynx	1.054	1.049	1.049	1.049	1.049	1.049	1.049	1.049
Lens	1.055	1.055	1.055	1.055	1.055	1.055	1.055	1.055
Liver	1.031	1.041	1.041	1.041	1.041	1.041	1.051	1.051
Lung	0.607	0.397	0.387	0.327	0.317	0.307	0.327	0.337
Muscle	1.042	1.040	1.040	1.040	1.040	1.040	1.040	1.040
Ovaries	1.044	1.043	1.043	1.043	1.043		1.043	
Pancreas	1.024	1.024	1.024	1.024	1.014	1.024	1.014	1.024
Pituitary gland	1.025	1.023	1.023	1.023	1.013	1.023	1.013	1.023
Prostate	1.025	1.023	1.023	1.023		1.023		1.023
Skin	1.092	1.088	1.088	1.088	1.088	1.088	1.088	1.088
Small intestine	1.024	1.024	1.024	1.024	1.024	1.024	1.024	1.024
Soft tissue Female	1.024	1.024	1.024	1.024	1.014		1.014	
Soft tissue Male	1.023	1.023	1.023	1.023		1.023	1.013	
Spleen	1.033	1.051	1.051	1.051	1.051	1.051	1.051	1.051

Organs/Tissues	00MF	01MF	05MF	10MF	15F	15M	ADF	ADM
Stomach	1.024	1.024	1.024	1.024	1.024	1.024	1.024	1.024
Teeth	1.500	1.500	1.500	2.113	2.727	2.727	2.727	2.727
Testes	1.034	1.034	1.034	1.034		1.034		1.034
Thymus	1.064	1.018	1.018	1.018	1.018	1.018	1.018	1.018
Thyroid	1.042	1.042	1.042	1.042	1.042	1.042	1.042	1.042
Tongue	1.042	1.040	1.040	1.040	1.040	1.040	1.040	1.040
Tonsils	1.025	1.023	1.023	1.023	1.013	1.023	1.013	1.023
Trachea	1.064	1.058	1.058	1.058	1.058	1.058	1.058	1.058
Urethra	1.025	1.023	1.023	1.023	1.023	1.023	1.023	1.023
Urinary bladder	1.033	1.033	1.033	1.033	1.033	1.033	1.033	1.033
Uterus	1.044	1.044	1.044	1.044	1.044		1.044	
Water	1.000	1.000	1.000	1.000	1.000	1.000	1.000	1.000
Air	0.001	0.001	0.001	0.001	0.001	0.001	0.001	0.001

Table 3

Electron density relative to water calculated for cortical and spongiosa (SP) bones included in the hybrid phantom series: 0-, 1-, 5-, 10-, 15-year-old, and adult (AD) male (M) and female (F).

Skeleton	00MF	01MF	05MF	10MF	15F	15M	ADF	ADM
Cortical bone	1.543	1.551	1.586	1.631	1.676	1.676	1.764	1.764
SP-Cranium	1.361	1.362	1.313	1.246	1.213	1.213	1.301	1.301
SP-Mandible	1.202	1.346	1.282	1.216	1.189	1.189	1.064	1.064
SP-Cervical Vertebrae	1.281	1.173	1.195	1.125	1.116	1.116	1.142	1.142
SP-Thoracic Vertebrae	1.293	1.139	1.145	1.095	1.095	1.095	1.080	1.080
SP-Lumbar Vertebrae	1.255	1.227	1.194	1.133	1.081	1.081	1.087	1.087
SP-Sternum	1.204	1.207	1.135	1.070	1.073	1.073	1.071	1.071
SP-Ribs	1.202	1.208	1.197	1.112	1.091	1.091	1.096	1.096
SP-Scapulae	1.214	1.238	1.214	1.148	1.204	1.204	1.112	1.112
SP-Clavicles	1.214	1.245	1.194	1.112	1.118	1.118	1.083	1.083
SP-Os coxae	1.214	1.177	1.157	1.103	1.077	1.077	1.076	1.076
SP-Sacrum	1.255	1.229	1.132	1.061	1.045	1.045	1.098	1.098
SP-Humeri, Proximal	1.255	1.303	1.246	1.189	1.106	1.106	1.065	1.065
SP-Humeri, Distal	1.255	1.303	1.234	1.164	1.128	1.128	1.098	1.098
SP-Radii, Proximal	1.255	1.311	1.155	1.126	1.122	1.122	1.051	1.051
SP-Radii, Distal	1.255	1.325	1.213	1.167	1.115	1.115	1.072	1.072
SP-Ulnae, Proximal	1.255	1.364	1.247	1.201	1.154	1.154	1.106	1.106
SP-Ulnae, Distal	1.255	1.247	1.092	1.079	1.108	1.108	1.089	1.089
SP-Wrists and Hands	1.202	1.234	1.191	1.113	1.064	1.064	1.098	1.098
SP-Femora, Proximal	1.255	1.286	1.245	1.197	1.140	1.140	1.105	1.105
SP-Femora, Distal	1.255	1.254	1.214	1.176	1.170	1.170	1.094	1.094
SP-Patellae	1.202	1.178	1.081	1.027	1.064	1.064	1.094	1.094
SP-Tibiae, Proximal	1.255	1.294	1.225	1.156	1.047	1.047	1.071	1.071
SP-Tibiae, Distal	1.255	1.269	1.133	1.106	1.108	1.108	1.078	1.078
SP-Fibulae, Proximal	1.255	1.307	1.153	1.118	1.085	1.085	1.043	1.043
SP-Fibulae, Distal	1.255	1.303	1.151	1.117	1.161	1.161	1.095	1.095
SP-Ankles and Feet	1.202	1.227	1.203	1.128	1.064	1.064	1.094	1.094

Skeleton	00MF	01MF	05MF	10MF	15F	15M	ADF	ADM
SP-Humeri, Upper Shaft	1.023	1.021	1.014	1.008	1.001	1.001	0.994	0.994
SP-Humeri, Lower Shaft	1.023	1.018	1.011	0.997	0.985	0.985	0.983	0.983
SP-Radii, Shaft	1.023	1.018	1.012	0.999	0.987	0.987	0.983	0.983
SP-Ulnae, Shaft	1.023	1.018	1.012	0.999	0.987	0.987	0.983	0.983
SP-Femora, Upper Shaft	1.023	1.021	1.014	1.008	1.001	1.001	0.994	0.994
SP-Femora, Lower Shaft	1.023	1.018	1.011	0.997	0.985	0.985	0.983	0.983
SP-Tibiae, Shaft	1.023	1.018	1.012	0.999	0.987	0.987	0.983	0.983
SP-Fibulae, Shaft	1.023	1.018	1.012	0.999	0.987	0.987	0.983	0.983

Table 4

Comparison of the electron density relative to water for selected organs between the original adult male hybrid phantom and the converted DICOM-image file in the Eclipse treatment planning system.

Organs	Relative electron density		
	Hybrid Phantom	Eclipse	Difference (%)
Lungs	0.337	0.335	-0.59
Thymus	1.018	1.017	-0.10
Spinal cord	1.035	1.039	0.39
Thyroid	1.042	1.041	-0.10
Spleen	1.051	1.050	-0.10
Trachea	1.058	1.057	-0.09
Ears	1.083	1.082	-0.09

Table 5

Comparison of organ volumes obtained from the original hybrid phantoms and the DICOM-structure files imported to the Eclipse system.

Phantoms	Organs or Tissues	Volume (cm^3)		Difference (%)
		Hybrid Phantom	Eclipse	
10-year Male	Brain	1259.55	1258.50	-0.08
	Thyroid	7.25	7.21	-0.55
	Eyeball	11.50	11.33	-1.48
Adult Male	Prostate	16.01	15.74	-1.69
	Urinary bladder	248.83	246.36	-0.99
	Testes	33.71	33.13	-1.72

Table 6

Comparison of average organ doses, and minimum and maximum point doses between the Eclipse and XVMC calculations in the 10-year-old and adult phantoms simulated for brain and prostate tumors, respectively.

10-year Male	**Average Dose (Gy)**		**Diff (%)**	**Max Point Dose (Gy)**		**Diff (%)**	**Min Point Dose (Gy)**		**Diff (%)**
	TPS	**MC**		**TPS**	**MC**		**TPS**	**MC**	
Brain	30.75	30.58	0.55	32.49	32.90	-1.26	23.74	24.10	-1.49
Brainstem	29.40	29.04	1.24	30.97	30.70	0.86	26.72	27.10	-1.42
Thyroid	0.54	0.56	-3.81	1.37	1.70	-19.71	0.31	0.30	1.67
Eyeballs	3.80	4.05	-6.10	16.23	13.90	16.73	1.58	2.10	-25.00
Adult Male	Average Dose (Gy)		Diff (%)	Max Point Dose (Gy)		Diff (%)	Min Point Dose (Gy)		Diff (%)
	TPS	MC		TPS	MC		TPS	MC	
Prostate	51.89	51.47	0.81	52.32	53.10	-1.48	50.35	48.70	3.38
Femoral Heads	17.81	17.76	0.28	52.21	53.30	-2.05	0.06	0.10	-45.00
Rectum	49.91	49.08	1.70	52.85	53.70	-1.59	16.35	15.30	6.83
Bladder	50.66	50.88	-0.43	52.36	53.70	-2.50	49.01	47.70	2.74
Testes	5.94	5.92	0.37	30.96	27.10	14.23	2.56	2.70	-5.37